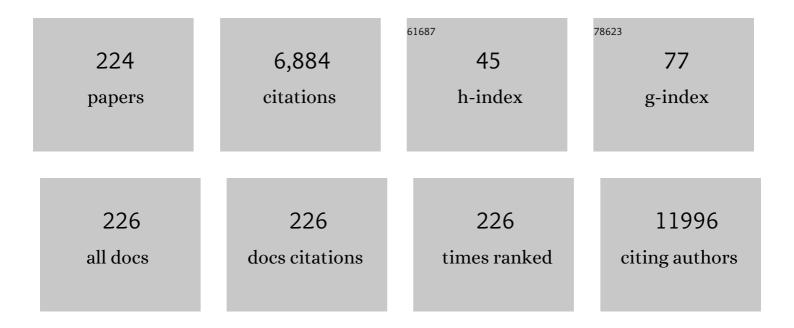
Gerd Duscher

List of Publications by Year in descending order

Source: https://exaly.com/author-pdf/3372195/publications.pdf Version: 2024-02-01



CEDD DUSCHED

#	Article	IF	CITATIONS
1	Selective Antisite Defect Formation in WS ₂ Monolayers via Reactive Growth on Dilute Wâ€Au Alloy Substrates. Advanced Materials, 2022, 34, e2106674.	11.1	14
2	Selective Antisite Defect Formation in WS ₂ Monolayers via Reactive Growth on Dilute Wâ€Au Alloy Substrates (Adv. Mater. 3/2022). Advanced Materials, 2022, 34, .	11.1	0
3	Aberration-corrected scanning transmission electron microscopy: the potential for nano- and interface science. International Journal of Materials Research, 2022, 94, 350-357.	0.1	0
4	Stabilized Synthesis of 2D Verbeekite: Monoclinic PdSe ₂ Crystals with High Mobility and In-Plane Optical and Electrical Anisotropy. ACS Nano, 2022, 16, 13900-13910.	7.3	14
5	Synthesis and characterization of amorphous Fe2.75Dy-oxide thin films demonstrating room-temperature semiconductor, magnetism, and optical transparency. Journal of Applied Physics, 2021, 129, 035701.	1.1	0
6	Direct Detection of Highly Localized Metal-Metal Interface Plasmons from Bimetallic Nanoparticles. Plasmonics, 2021, 16, 957-964.	1.8	4
7	Explosive vaporization of metallic nanostructures on a surface by nanosecond laser heating under fluids. Journal of Applied Physics, 2021, 129, .	1.1	3
8	Strain-Induced Growth of Twisted Bilayers during the Coalescence of Monolayer MoS ₂ Crystals. ACS Nano, 2021, 15, 4504-4517.	7.3	19
9	Understanding Substrate-Guided Assembly in van der Waals Epitaxy by <i>in Situ</i> Laser Crystallization within a Transmission Electron Microscope. ACS Nano, 2021, 15, 8638-8652.	7.3	7
10	Bimetallic Fe–Ag Nanopyramid Arrays for Optical Communication Applications. ACS Applied Nano Materials, 2021, 4, 5758-5767.	2.4	3
11	Atomic structures of interfacial solute gateways to Î,′ precipitates in Al-Cu alloys. Acta Materialia, 2021, 212, 116891.	3.8	18
12	Excitonic Dynamics in Janus MoSSe and WSSe Monolayers. Nano Letters, 2021, 21, 931-937.	4.5	86
13	Versatile Tunability of the Metal Insulator Transition in (TiO ₂) <i>_m</i> /(VO ₂) <i>_m</i> Superlattices. Advanced Functional Materials, 2020, 30, 2004914.	7.8	4
14	Nonâ€Equilibrium Synthesis of Highly Active Nanostructured, Oxygenâ€Incorporated Amorphous Molybdenum Sulfide HER Electrocatalyst. Small, 2020, 16, e2004047.	5.2	29
15	In Situ Laser Synthesis of 2D WSe2 Within TEM. Microscopy and Microanalysis, 2020, 26, 1120-1121.	0.2	0
16	Nanosecond switchable localized surface plasmons through resettable contact angle behavior in silver nanoparticles. Nanotechnology, 2020, 31, 355503.	1.3	2
17	2D Materials: Twoâ€Dimensional Palladium Diselenide with Strong Inâ€Plane Optical Anisotropy and High Mobility Grown by Chemical Vapor Deposition (Adv. Mater. 19/2020). Advanced Materials, 2020, 32, 2070152.	11.1	2
18	Twoâ€Dimensional Palladium Diselenide with Strong Inâ€Plane Optical Anisotropy and High Mobility Grown by Chemical Vapor Deposition. Advanced Materials, 2020, 32, e1906238.	11,1	81

Gerd Duscher

0

#	Article	IF	CITATIONS
19	Low Energy Implantation into Transition-Metal Dichalcogenide Monolayers to Form Janus Structures. ACS Nano, 2020, 14, 3896-3906.	7.3	136
20	Integration of amorphous ferromagnetic oxides with multiferroic materials for room temperature magnetoelectric spintronics. Scientific Reports, 2020, 10, 3583.	1.6	16
21	In situ laser reflectivity to monitor and control the nucleation and growth of atomically thin 2D materials*. 2D Materials, 2020, 7, 025048.	2.0	14
22	Binary Oxide Superlattices: Versatile Tunability of the Metal Insulator Transition in (TiO ₂) <i>_m</i> (VO ₂) <i>_m</i> Superlattices (Adv.) Tj ETQq(D 0⁻.8 rgBT	/Øverlock 10
23	Continuous Wave Resonant Photon Stimulated Electron Energy-Gain and Electron Energy-Loss Spectroscopy of Individual Plasmonic Nanoparticles. ACS Photonics, 2019, 6, 2499-2508.	3.2	25
24	Recent progress in characterization of the core–shell structure of black titania. Journal of Materials Research, 2019, 34, 1138-1153.	1.2	15
25	Direct imaging of the nitrogen-rich edge in monolayer hexagonal boron nitride and its band structure tuning. Nanoscale, 2019, 11, 20676-20684.	2.8	10
26	Measuring the areal density of nanomaterials by electron energy-loss spectroscopy. Ultramicroscopy, 2019, 196, 154-160.	0.8	7
27	Graphitic coated Al nanoparticles manufactured as superior energetic materials via laser ablation synthesis in organic solvents. Applied Surface Science, 2019, 473, 156-163.	3.1	44
28	Feature extraction via similarity search: application to atom finding and denoising in electron and scanning probe microscopy imaging. Advanced Structural and Chemical Imaging, 2018, 4, 3.	4.0	31
29	High-performance multilayer WSe2 field-effect transistors with carrier type control. Nano Research, 2018, 11, 722-730.	5.8	101
30	Mapping the layer count of few-layer hexagonal boron nitride at high lateral spatial resolutions. 2D Materials, 2018, 5, 015007.	2.0	8

31	Exploring Photothermal Pathways via in Situ Laser Heating in the Transmission Electron Microscope: Recrystallization, Grain Growth, Phase Separation, and Dewetting in Ag0.5Ni0.5 Thin Films. Microscopy and Microanalysis, 2018, 24, 647-656.	0.2	21
32	Laser Synthesis, Processing, and Spectroscopy of Atomically-Thin Two Dimensional Materials. Springer Series in Materials Science, 2018, , 1-37.	0.4	1
33	Multiscale characterization of irradiation behaviour of ion-irradiated SiC/SiC composites. Acta Materialia, 2018, 161, 207-220.	3.8	36
34	Tungsten Diselenide Patterning and Nanoribbon Formation by Gasâ€Assisted Focusedâ€Heliumâ€Ionâ€Beamâ€Induced Etching. Small Methods, 2017, 1, 1600060.	4.6	33
35	High efficiency core-loss EELS analyzing from the viewpoint of chemometrics. Materials Characterization, 2017, 129, 313-318.	1.9	1

New approaches for synthesis and processing of 2D materials (Conference Presentation)., 2017,,.

3

#	Article	IF	CITATIONS
37	Transition Metal Dichalcogenides: Suppression of Defects and Deep Levels Using Isoelectronic Tungsten Substitution in Monolayer MoSe ₂ (Adv. Funct. Mater. 19/2017). Advanced Functional Materials, 2017, 27, .	7.8	3
38	Black Anatase Formation by Annealing of Amorphous Nanoparticles and the Role of the Ti ₂ O ₃ Shell in Self-Organized Crystallization by Particle Attachment. ACS Applied Materials & Interfaces, 2017, 9, 22018-22025.	4.0	15
39	Correlating the optical properties of WS2 monolayers grown by CVD with isoelectronic Mo doping level (Conference Presentation). , 2017, , .		0
40	Emission dynamics of hybrid plasmonic gold/organic GaN nanorods. Nanotechnology, 2017, 28, 505710.	1.3	6
41	Layer Count Mapping of Multilayer Hexagonal Boron Nitride Thin Films. Microscopy and Microanalysis, 2017, 23, 412-413.	0.2	0
42	High Conduction Hopping Behavior Induced in Transition Metal Dichalcogenides by Percolating Defect Networks: Toward Atomically Thin Circuits. Advanced Functional Materials, 2017, 27, 1702829.	7.8	52
43	Experimentally determined edge orientation of triangular crystals of hexagonal boron nitride. Physica Status Solidi (B): Basic Research, 2017, 254, 1700069.	0.7	13
44	Bottom up synthesis of boron-doped graphene for stable intermediate temperature fuel cell electrodes. Carbon, 2017, 123, 605-615.	5.4	23
45	Surface Mechanoengineering of a Zr-Based Bulk Metallic Glass via Ar-Nanobubble Doping To Probe Cell Sensitivity to Rigid Materials. ACS Applied Materials & Interfaces, 2017, 9, 43429-43437.	4.0	7
46	Nonequilibrium Synthesis of TiO ₂ Nanoparticle "Building Blocks―for Crystal Growth by Sequential Attachment in Pulsed Laser Deposition. Nano Letters, 2017, 17, 4624-4633.	4.5	33
47	Suppression of Defects and Deep Levels Using Isoelectronic Tungsten Substitution in Monolayer MoSe ₂ . Advanced Functional Materials, 2017, 27, 1603850.	7.8	84
48	Quantification of Low Voltage Images of 2-dimensional Materials in Aberration Corrected Scanning Transmission Electron Microscopy Microscopy and Microanalysis, 2017, 23, 464-465.	0.2	0
49	Mapping Giant Oscillator Excitons in Semiconducting Nano Wires. Microscopy and Microanalysis, 2017, 23, 374-375.	0.2	0
50	Atomic Structure and Properties of Dislocations and Grain Boundaries. , 2016, , .		0
51	Controlling the exciton emission of gold coated GaAs–AlGaAs core–shell nanowires with an organic spacer layer. Nanotechnology, 2016, 27, 485204.	1.3	9
52	Exciton emission from plasmonic-organic-IIIâ \in "V-semiconductor nanowires and nanorods. , 2016, , .		0
53	Dose dependence of helium bubble formation in nano-engineered SiC at 700°C. Journal of Nuclear Materials, 2016, 472, 153-160.	1.3	26
54	Focused helium-ion beam irradiation effects on electrical transport properties of few-layer WSe2: enabling nanoscale direct write homo-junctions. Scientific Reports, 2016, 6, 27276.	1.6	99

#	Article	IF	CITATIONS
55	Tailoring Vacancies Far Beyond Intrinsic Levels Changes the Carrier Type and Optical Response in Monolayer MoSe _{2â^'<i>x</i>} Crystals. Nano Letters, 2016, 16, 5213-5220.	4.5	121
56	Observation of Nanoscale Morphological and Structural Degradation in Perovskite Solar Cells by in Situ TEM. ACS Applied Materials & amp; Interfaces, 2016, 8, 32333-32340.	4.0	54
57	Interlayer Coupling in Twisted WSe ₂ /WS ₂ Bilayer Heterostructures Revealed by Optical Spectroscopy. ACS Nano, 2016, 10, 6612-6622.	7.3	249
58	Ultrathin GaN quantum disk nanowire LEDs with sub-250 nm electroluminescence. Nanoscale, 2016, 8, 8024-8032.	2.8	44
59	Tandem laser ablation synthesis in solution-galvanic replacement reaction (LASiS-GRR) for the production of PtCo nanoalloys as oxygen reduction electrocatalysts. Journal of Power Sources, 2016, 306, 413-423.	4.0	63
60	Novel Iron-Based Amorphous Transparent Conducting Oxide. , 2016, , .		0
61	Ferroplasmons: Novel Plasmons in Metal-Ferromagnetic Bimetallic Nanostructures. Microscopy and Microanalysis, 2015, 21, 2381-2382.	0.2	2
62	Nanoscopic imaging of energy transfer from single plasmonic particles to semiconductor substrates via STEM/EELS. Microscopy and Microanalysis, 2015, 21, 1909-1910.	0.2	0
63	Novel Iron-based ternary amorphous oxide semiconductor with very high transparency, electronic conductivity and mobility. Scientific Reports, 2015, 5, 18157.	1.6	9
64	Controllable Growth of Perovskite Films by Roomâ€Temperature Air Exposure for Efficient Planar Heterojunction Photovoltaic Cells. Angewandte Chemie - International Edition, 2015, 54, 14862-14865.	7.2	41
65	Laser-Induced Self-Assembled Nanostructures on Electron-Transparent Substrates. Particle and Particle Systems Characterization, 2015, 32, 476-482.	1.2	10
66	Peculiar Plasmon Peak Position in Electron Energy Loss Spectrum of Hexagonal Boron Nitride/Graphene Double Layer. Microscopy and Microanalysis, 2015, 21, 985-986.	0.2	5
67	Twoâ€Dimensionally Ordered Plasmonic and Magnetic Nanostructures on Transferable Electronâ€Transparent Substrates. Particle and Particle Systems Characterization, 2015, 32, 970-978.	1.2	9
68	Quantitative Phase Fraction Detection in Organic Photovoltaic Materials through EELS Imaging. Polymers, 2015, 7, 2446-2460.	2.0	16
69	Characterization of Sulfonated Polysulfone Polymers by EELS. Microscopy and Microanalysis, 2015, 21, 1679-1680.	0.2	0
70	Combine Simulation and Experiment EELS to Characterize Ionomer Conformation. Microscopy and Microanalysis, 2015, 21, 1653-1654.	0.2	1
71	Perovskite Solar Cells with Near 100% Internal Quantum Efficiency Based on Large Single Crystalline Grains and Vertical Bulk Heterojunctions. Journal of the American Chemical Society, 2015, 137, 9210-9213.	6.6	246
72	Correlating high power conversion efficiency of PTB7:PC ₇₁ BM inverted organic solar cells with nanoscale structures. Nanoscale, 2015, 7, 15576-15583.	2.8	54

#	Article	IF	CITATIONS
73	Localized surface plasmon sensing based investigation of nanoscale metal oxidation kinetics. Nanotechnology, 2015, 26, 205701.	1.3	10
74	Exciton emission from hybrid organic and plasmonic polytype InP nanowire heterostructures. Materials Research Express, 2015, 2, 045001.	0.8	6
75	Spatially Mapping Energy Transfer from Single Plasmonic Particles to Semiconductor Substrates via STEM/EELS. Nano Letters, 2015, 15, 3465-3471.	4.5	77
76	Structure and Formation Mechanism of Black TiO ₂ Nanoparticles. ACS Nano, 2015, 9, 10482-10488.	7.3	170
77	Characterization of chain conformations in perfluorosulfonic acid membranes using electron energy loss spectroscopy. RSC Advances, 2015, 5, 2368-2373.	1.7	15
78	Structure characterization and strain relief analysis in CVD growth of boron phosphide on silicon carbide. Applied Surface Science, 2015, 327, 7-12.	3.1	36
79	Electron energy loss spectroscopy of polytetrafluoroethylene: experiment and first principles calculations. Microscopy (Oxford, England), 2014, 63, 73-83.	0.7	19
80	Anti-Site Defects in Perovskite YAlO3:Ce Using Aberration-Corrected STEM. Microscopy and Microanalysis, 2014, 20, 132-133.	0.2	2
81	Roughness of the SiC/SiO2 vicinal interface and atomic structure of the transition layers. Journal of Vacuum Science and Technology A: Vacuum, Surfaces and Films, 2014, 32, .	0.9	13
82	Catalytic nanoparticles for carbon nanotube growth synthesized by through thin film femtosecond laser ablation. Proceedings of SPIE, 2014, , .	0.8	1
83	Focused helium and neon ion beam induced etching for advanced extreme ultraviolet lithography mask repair. Journal of Vacuum Science and Technology B:Nanotechnology and Microelectronics, 2014, 32, .	0.6	28
84	Unusual role of epilayer–substrate interactions in determining orientational relations in van der Waals epitaxy. Proceedings of the National Academy of Sciences of the United States of America, 2014, 111, 16670-16675.	3.3	64
85	Pulsed Laser Deposition of Photoresponsive Twoâ€Đimensional GaSe Nanosheet Networks. Advanced Functional Materials, 2014, 24, 6365-6371.	7.8	108
86	The impact of selective solvents on the evolution of structure and function in solvent annealed organic photovoltaics. RSC Advances, 2014, 4, 27931-27938.	1.7	18
87	Digital Transfer Growth of Patterned 2D Metal Chalcogenides by Confined Nanoparticle Evaporation. ACS Nano, 2014, 8, 11567-11575.	7.3	47
88	Ferroplasmons: Intense Localized Surface Plasmons in Metal-Ferromagnetic Nanoparticles. ACS Nano, 2014, 8, 9790-9798.	7.3	46
89	Guided crystallization of P3HT in ternary blend solar cell based on P3HT:PCPDTBT:PCBM. Energy and Environmental Science, 2014, 7, 3782-3790.	15.6	60
90	Universal Formation of Compositionally Graded Bulk Heterojunction for Efficiency Enhancement in Organic Photovoltaics. Advanced Materials, 2014, 26, 3068-3075.	11.1	139

#	Article	IF	CITATIONS
91	Chemical composition study of high- <i>k</i> La-silicate gate stacks at sub-nanometer scale. Physica Status Solidi (A) Applications and Materials Science, 2014, 211, 2537-2540.	0.8	1
92	Electron Energy-Loss Spectroscopic Imaging for Phase Detection in Organic Photovoltaics. Microscopy and Microanalysis, 2014, 20, 538-539.	0.2	0
93	Direct Observation of Defects in Hexagonal Boron Nitride Monolayers. Microscopy and Microanalysis, 2014, 20, 1738-1739.	0.2	2
94	Laser Interactions for the Synthesis and In Situ Diagnostics of Nanomaterials. Springer Series in Materials Science, 2014, , 143-173.	0.4	4
95	Oxidationâ€Resistant Silver Nanostructures for Ultrastable Plasmonic Applications. Advanced Materials, 2013, 25, 2045-2050.	11.1	51
96	Synthesis of Millimeter-Size Hexagon-Shaped Graphene Single Crystals on Resolidified Copper. ACS Nano, 2013, 7, 8924-8931.	7.3	178
97	Evaluation of the microstructure of dry and hydrated perfluorosulfonic acid ionomers: microscopy and simulations. Journal of Materials Chemistry A, 2013, 1, 938-944.	5.2	39
98	High-temperature transformation of Fe-decorated single-wall carbon nanohorns to nanooysters: a combined experimental and theoretical study. Nanoscale, 2013, 5, 1849-1857.	2.8	10
99	Direct observation of dislocation dissociation and Suzuki segregation in a Mg–Zn–Y alloy by aberration-corrected scanning transmission electron microscopy. Acta Materialia, 2013, 61, 350-359.	3.8	126
100	Enhanced absorption in ultrathin Si by NiSi ₂ nanoparticles. Nanomaterials and Energy, 2013, 2, 11-19.	0.1	7
101	Plasmon Excitations in Bimetallic Ag Nanostructures by Monochromated E-Beam. Microscopy and Microanalysis, 2013, 19, 1510-1511.	0.2	3
102	Self-organized bimetallic Ag–Co nanoparticles with tunable localized surface plasmons showing high environmental stability and sensitivity. Nanotechnology, 2012, 23, 275604.	1.3	55
103	Absorption enhancement by Ni-silicide nanostructures embedded in ultra-thin Si films. Microscopy and Microanalysis, 2012, 18, 1862-1863.	0.2	0
104	Nanoporous Carbon: Topological Defects: Origin of Nanopores and Enhanced Adsorption Performance in Nanoporous Carbon (Small 21/2012). Small, 2012, 8, 3282-3282.	5.2	3
105	Oxidation Resistance of Reactive Atoms in Graphene. Nano Letters, 2012, 12, 4651-4655.	4.5	64
106	Topological Defects: Origin of Nanopores and Enhanced Adsorption Performance in Nanoporous Carbon. Small, 2012, 8, 3283-3288.	5.2	139
107	The effect of zirconium implantation on the structure of sapphire. Nuclear Instruments & Methods in Physics Research B, 2012, 286, 190-195.	0.6	3
108	Nonequilibrium laser synthesis and real-time diagnostics of carbon nanomaterial growth. , 2012, , .		0

#	Article	IF	CITATIONS
109	Scanning transmission electron microscope observations of defects in as-grown and pre-strained Mo alloy fibers. Acta Materialia, 2011, 59, 2172-2179.	3.8	37
110	Quantum stability and superconducting properties of ultrathin alloy films made from bulk immiscible elements: Pb and Ga. Physical Review B, 2011, 84, .	1.1	3
111	Optimization of homoepitaxially grown AlGaN/GaN heterostructures. Physica Status Solidi (A) Applications and Materials Science, 2010, 207, 2292-2299.	0.8	4
112	Excess carbon in silicon carbide. Journal of Applied Physics, 2010, 108, 123705.	1.1	26
113	Carbon Clusters as Possible Defects in the SiC–SiO ₂ Interface. Journal of Computational and Theoretical Nanoscience, 2009, 6, 1305-1310.	0.4	4
114	Reliable Quantification of EELS Spectra with a Simple Model–Based Approach. Microscopy and Microanalysis, 2009, 15, 446-447.	0.2	4
115	Relationship between 4H-SiCâ^•SiO2 transition layer thickness and mobility. Applied Physics Letters, 2009, 95, 032108.	1.5	85
116	Threeâ€Dimensional Geometry of Nanometerâ€Scale AlN Pits: A New Template for Quantum Dots?. Advanced Materials, 2008, 20, 134-137.	11.1	5
117	Direct Observation of Inversion Domain Boundaries of GaN on <i>c</i> apphire at Subâ€Ã¥ngstrom Resolution. Advanced Materials, 2008, 20, 2162-2165.	11.1	31
118	Detailed arsenic concentration profiles at Si/SiO2 interfaces. Journal of Applied Physics, 2008, 104, 043507.	1.1	20
119	Distribution and segregation of arsenic at theSiO2/Si interface. Journal of Applied Physics, 2008, 104, 023518.	1.1	25
120	Transition layers at the SiO2â^•SiC interface. Applied Physics Letters, 2008, 93, .	1.5	140
121	Interfacial and Solvent Effects Govern the Formation of Tris(dibenzylidenacetone)dipalladium(0) Microstructures. Langmuir, 2008, 24, 7803-7809.	1.6	14
122	Self-assembled three-dimensional Cu–Ge nanoweb composite. Nanotechnology, 2008, 19, 135603.	1.3	7
123	Characterization of the origin of band states in the SiC/SiO ₂ interface. , 2007, , .		0
124	Chemical composition changes across the interface of amorphous LaScO3 on Si (001). Applied Physics Letters, 2007, 91, 152901.	1.5	2
125	Thermal annealing effect on the interface structure of high-κ LaScO3 on silicon. Applied Physics Letters, 2007, 91, 152906.	1.5	4
126	Quantitative nanoscale local strain profiling in embedded SiGe metal-oxide-semiconductor structures. Applied Physics Letters, 2007, 90, 191907.	1.5	10

#	Article	IF	CITATIONS
127	Characterization of the Segregation of Arsenic at the Interface SiO ₂ /Si. Materials Research Society Symposia Proceedings, 2007, 994, 1.	0.1	4
128	The mechanism for polarity inversion of GaN via a thin AlN layer: Direct experimental evidence. Applied Physics Letters, 2007, 91, 203115.	1.5	59
129	Transmission electron microscopy studies of regrown GaN Ohmic contacts on patterned substrates for metal oxide semiconductor field effect transistor applications. Applied Physics Letters, 2007, 90, 204106.	1.5	16
130	The Role of Selection Pressure in RNA-Mediated Evolutionary Materials Synthesis. Journal of the American Chemical Society, 2007, 129, 15340-15346.	6.6	18
131	Characterization of the pile-up of As at the SiO <inf>2</inf> /Si interface. , 2007, , .		2
132	Gold and Silica-Coated Gold Nanoparticles as Thermographic Labels for DNA Detection. Analytical Chemistry, 2006, 78, 3282-3288.	3.2	63
133	Reliable Local Strain Characterization on Si/SiGe Structures in Biaxial Tension. Materials Research Society Symposia Proceedings, 2006, 958, 1.	0.1	1
134	Atomic level imaging of Au nanocluster dispersed in TiO2 and SrTiO3. Nuclear Instruments & Methods in Physics Research B, 2006, 242, 380-382.	0.6	9
135	Effect of Pb on the mechanical properties of nanocrystalline Al. Scripta Materialia, 2006, 55, 155-158.	2.6	34
136	Si/SiO ₂ and SiC/SiO ₂ Interfaces for MOSFETs – Challenges and Advances. Materials Science Forum, 2006, 527-529, 935-948.	0.3	54
137	Surface plasmon resonance in conducting metal oxides. Journal of Applied Physics, 2006, 100, 054905.	1.1	258
138	Atomic Resolution Imaging of Au Nanocluster Dispersed in TiO2, SrTiO3, and MgO. Journal of the American Ceramic Society, 2005, 88, 3184-3191.	1.9	7
139	A new understanding of near-threshold damage for 200 keV irradiation in silicon. Journal of Materials Science, 2005, 40, 3639-3650.	1.7	6
140	Role of Fe and Ni Nanoparticles on Mechanical Properties of Alumina Thin Films deposited by Laser Ablation. Materials Research Society Symposia Proceedings, 2005, 890, 1.	0.1	0
141	Self-assembling of nanocavities inTiO2dispersed with Au nanoclusters. Physical Review B, 2005, 72, .	1.1	5
142	Segregation and enhanced diffusion of nitrogen in silicon induced by low energy ion bombardment. Journal of Applied Physics, 2005, 97, 083534.	1.1	4
143	Low-Temperature Resistance Anomaly atSrTiO3Grain Boundaries: Evidence for an Interface-Induced Phase Transition. Physical Review Letters, 2005, 95, 197601.	2.9	23
144	AbÂlnitioldentification of the Nitrogen Diffusion Mechanism in Silicon. Physical Review Letters, 2005, 95, 025901.	2.9	28

#	Article	IF	CITATIONS
145	Direct imaging of quantum antidots in MgO dispersed with Au nanoclusters. Applied Physics Letters, 2005, 87, 153104.	1.5	8
146	Void formation during early stages of passivation: Initial oxidation of iron nanoparticles at room temperature. Journal of Applied Physics, 2005, 98, 094308.	1.1	238
147	Direct observation of substitutional Au atoms inSrTiO3. Physical Review B, 2004, 70, .	1.1	6
148	Precipitation of Au nanoclusters in SrTiO3 by ion implantation. Journal of Applied Physics, 2004, 95, 5060-5068.	1.1	11
149	"Umbrella―like precipitates in nitrogen-doped Czochralski silicon wafers. Applied Physics Letters, 2004, 84, 1889-1891.	1.5	3
150	Simulation and Electron Energy-Loss Spectroscopy of Electron Beam Induced Point Defect Agglomerations in Silicon. Materials Research Society Symposia Proceedings, 2004, 810, 178.	0.1	1
151	Bismuth-induced embrittlement of copper grain boundaries. Nature Materials, 2004, 3, 621-626.	13.3	242
152	Copper Segregation to the Â5 (310)/[001] Symmetric Tilt Grain Boundary in Aluminum. Journal of Materials Science, 2004, 12, 165-174.	1.2	19
153	Modeling and characterization of atomically sharp "perfect―Ge/SiO2 interfaces. Materials Science and Engineering B: Solid-State Materials for Advanced Technology, 2004, 114-115, 156-161.	1.7	10
154	Microstructure of precipitated Au nanoclusters in TiO2. Journal of Applied Physics, 2004, 95, 8185-8193.	1.1	24
155	Investigation of Nanostructured Germanium/Silicon Dioxide Interfaces. Journal of Computational and Theoretical Nanoscience, 2004, 1, 286-295.	0.4	1
156	Nano-scale analysis of precipitates in nitrogen-doped Czochralski silicon. Microelectronic Engineering, 2003, 66, 305-313.	1.1	8
157	Investigation of the detailed structure of atomically sharp Ge/SiO/sub 2/ interfaces. , 2003, , .		2
158	In Situ Point Defect Generation and Agglomeration during Electron-Beam Irradiation of Nitrogen-Doped Czochralski Silicon. Electrochemical and Solid-State Letters, 2003, 6, G134.	2.2	6
159	Formation of nanoscale voids and related metallic impurity gettering in high-energy ion-implanted and annealed epitaxial silicon. Applied Physics Letters, 2003, 83, 1367-1369.	1.5	11
160	Plasma plume characteristics and properties of pulsed laser deposited diamond-like carbon films. Journal of Applied Physics, 2003, 93, 3627-3634.	1.1	34
161	Effect of microstructure on diffusion of copper in TiN films. Journal of Applied Physics, 2003, 93, 5210-5214.	1.1	32
162	Transmission Electron Microscopy: Overview and Challenges. AIP Conference Proceedings, 2003, , .	0.3	4

#	Article	IF	CITATIONS
163	Aberration-Corrected Scanning Transmission Electron Microscopy: The Potential for Nano- and Interface Science. International Journal of Materials Research, 2003, 94, 350-357.	0.8	18
164	Atomic Resolution Z-contrast Imaging and EELS: Application for Ge/SiO2 Interface. Microscopy and Microanalysis, 2003, 9, 818-819.	0.2	0
165	Atomistic Modeling of the Detailed Structure of Si/SiO2 Interfaces Using AIDATEM (Ab-initio Interface) Tj ETQq1 9, 826-827.	0.78431 0.2	4 rgBT /Ov <mark>er</mark> 0
166	Z-contrast imaging of dislocation cores at the GaAs/Si interface. Applied Physics Letters, 2002, 81, 2728-2730.	1.5	40
167	Z-contrast Imaging and EELS of Dislocation Cores at the Si/GaAs Interface. Materials Research Society Symposia Proceedings, 2002, 744, 1.	0.1	0
168	Synthesis and atomic-level characterization of Ni nanoparticles in Al2O3 matrix. Applied Physics Letters, 2002, 81, 4204-4206.	1.5	32
169	The Local Electronic structure at Grain Boundaries and Hetero- Interfaces in ZnO Thin Films Grown by Laser Deposition Materials Research Society Symposia Proceedings, 2002, 727, 1.	0.1	2
170	STEM Investigations of Defects and Interfaces In Complex Oxides. Microscopy and Microanalysis, 2002, 8, 384-385.	0.2	0
171	Z-Contrast Imaging of Dislocation Cores at the Si/GaAs Interface. Microscopy and Microanalysis, 2002, 8, 1604-1605.	0.2	0
172	Cu, Nb and V on (110) TiO2 (rutile): epitaxy and chemical reactions. Thin Solid Films, 2001, 398-399, 419-426.	0.8	19
173	Core Hole Effects on Eels Near-Edge Fine Structure in Semiconductors and Insulators. Microscopy and Microanalysis, 2001, 7, 1174-1175.	0.2	0
174	Non-Stoichiometry at Dislocation Cores in Perovskites and Related Materials. Microscopy and Microanalysis, 2001, 7, 306-307.	0.2	0
175	The Si/SiO2 Interface: Atomic Structures, Composition, Strain and Energetics. Microscopy and Microanalysis, 2001, 7, 768-769.	0.2	0
176	Diffusion Characteristics of Cu in TiN Thin Films. Materials Research Society Symposia Proceedings, 2001, 686, 1.	0.1	0
177	Critical Currents at Grain Boundaries in High Temperature Superconductors. Materials Research Society Symposia Proceedings, 2001, 689, 1.	0.1	0
178	Core-hole effects on energy-loss near-edge structure. Ultramicroscopy, 2001, 86, 355-362.	0.8	65
179	Consequence of Nanometerâ€Scale Property Variations to Macroscopic Properties of CrOCN Thin Films. Journal of the American Ceramic Society, 2001, 84, 2873-2881.	1.9	7
180	Nonstoichiometry and the Electrical Activity of Grain Boundaries inSrTiO3. Physical Review Letters, 2001, 86, 4056-4059.	2.9	176

#	Article	IF	CITATIONS
181	Local and Global Bonding at the Si-SiO2 Interface. Springer Series in Materials Science, 2001, , 193-218.	0.4	6
182	Dislocations in Semiconductors: Atomic Structure and Properties. , 2001, , 2312-2325.		0
183	The Origin of Electrical Activity at Grain Boundaries in Perovskites and Related Materials. Materials Research Society Symposia Proceedings, 2000, 654, 131.	0.1	0
184	Bonding, Defects, And Defect Dynamics In The Sic-SiO2 System. Materials Research Society Symposia Proceedings, 2000, 640, 1.	0.1	2
185	The Electronic Structure of Pristine and Doped (100) Tilt Grain Boundaries in SrTiO3. Journal of Materials Science, 2000, 8, 199-208.	1.2	16
186	Non-Stoichiometry at Tilt Grain Boundaries in SrTiO3. Microscopy and Microanalysis, 2000, 6, 114-115.	0.2	1
187	The Role of Non-Stoichiometry in the Electrical Activity of Grain Boundaries in SrTiO3. Microscopy and Microanalysis, 2000, 6, 184-185.	0.2	0
188	Excitonic Effects in Core-Excitation Spectra of Semiconductors. Physical Review Letters, 2000, 85, 2168-2171.	2.9	76
189	Cathodoluminescent properties at nanometer resolution through Z-contrast scanning transmission electron microscopy. Applied Physics Letters, 2000, 77, 594-596.	1.5	8
190	Fe ₁₆ Al ₁₄ B ₂ phase in Fe–Al alloys. Philosophical Magazine A: Physics of Condensed Matter, Structure, Defects and Mechanical Properties, 2000, 80, 2737-2745.	0.8	6
191	Atomic-Scale Engineering of the SiC-SiO ₂ Interface. Materials Science Forum, 2000, 338-342, 1133-1136.	0.3	9
192	Nb on (110) TiO2 (rutile): growth, structure, and chemical composition of the interface. Surface Science, 2000, 446, 219-228.	0.8	24
193	The Si/SiO ₂ Interface: Atomic Structures, Composition, Strain And Energetics. Microscopy and Microanalysis, 1999, 5, 122-123.	0.2	3
194	Decomposition of the ZrO2 electrolyte in contact with Ni: Structure and chemical composition of the Ni–electrolyte interface. Journal of Materials Research, 1999, 14, 3340-3345.	1.2	8
195	The influence of atomic structure on the formation of electrical barriers at grain boundaries in SrTiO3. Applied Physics Letters, 1999, 74, 2638-2640.	1.5	90
196	Electronic structure of a grain-boundary model inSrTiO3. Physical Review B, 1999, 60, 2416-2424.	1.1	86
197	A combined experimental and theoretical approach to grain boundary structure and segregation. Physica B: Condensed Matter, 1999, 273-274, 453-457.	1.3	15
198	Investigating the atomic scale structure and chemistry of grain boundaries in high- T c superconductors. Micron, 1999, 30, 425-436.	1.1	19

Gerd Duscher

#	Article	IF	CITATIONS
199	Silicon and zinc telluride nanoparticles synthesized by low energy density pulsed laser ablation into ambient gases. Journal of Materials Research, 1999, 14, 359-370.	1.2	48
200	Correlating Atomic Scale Experimental Observations to Develop Three-Dimensional Structural Models for Grain Boundaries in Oxides. Microscopy and Microanalysis, 1999, 5, 48-57.	0.2	3
201	Atomic-Resolution Z-Contrast Imaging and its Application to Compositional Ordering and Segregation. Materials Research Society Symposia Proceedings, 1999, 583, 235.	0.1	Ο
202	Microscopic and Theoretical Investigations of the Si-SiO2 Interface. Materials Research Society Symposia Proceedings, 1999, 592, 42.	0.1	1
203	Investigating the Structureâ€Property Relationships at Grain Boundaries in MgO Using Bondâ€Valence Pair Potentials and Multiple Scattering Analysis. Journal of the American Ceramic Society, 1999, 82, 366-372.	1.9	8
204	Investigation of the local superconducting properties in Ag-sheathed BSCCO tapes by STEM. Physica C: Superconductivity and Its Applications, 1998, 298, 1-9.	0.6	6
205	Atomic Column Resolved Electron Energy-Loss Spectroscopy. Physica Status Solidi A, 1998, 166, 327-342.	1.7	84
206	Silicon and zinc telluride nanoparticles synthesized by pulsed laser ablation: size distributions and nanoscale structure. Applied Surface Science, 1998, 127-129, 355-361.	3.1	51
207	Time-resolved imaging of gas phase nanoparticle synthesis by laser ablation. Applied Physics Letters, 1998, 72, 2987-2989.	1.5	318
208	Photoluminescence from gas-suspended SiOx nanoparticles synthesized by laser ablation. Applied Physics Letters, 1998, 73, 438-440.	1.5	108
209	Impurity-Induced Structural Transformation of a MgO Grain Boundary. Physical Review Letters, 1998, 81, 3675-3678.	2.9	108
210	Atomic structure of a Ca-doped [001] tilt grain boundary in MgO. Journal of Electron Microscopy, 1998, 47, 115-120.	0.9	12
211	Time-Resolved Imaging and Photoluminescence of Gas-Suspended Nanoparticles Synthesized by Laser Ablation: Dynamics, Transport, Collection, and Ex Situ Analysis. Materials Research Society Symposia Proceedings, 1998, 526, 47.	0.1	1
212	In Situ Diagnostics of Nanomaterial Synthesis by Laser Ablation: Time-resolved Photoluminescence Spectra and Imaging of Gas-Suspended Nanoparticles Deposited for Thin Films. Materials Research Society Symposia Proceedings, 1998, 536, 359.	0.1	0
213	Atomic Scale Structure-Property Relationships of Defects and Interfaces in Ceramics. Microscopy and Microanalysis, 1998, 4, 556-557.	0.2	0
214	Investigation of the Local Superconducting Properties at Grain Boundaries in High-Tc Superconductors. Microscopy and Microanalysis, 1998, 4, 690-691.	0.2	0
215	Investigating Ca Segregated to a Grain Boundaries in MgO Using Multiple Scattering Analysis of Electron Energy Loss Spectra. Microscopy and Microanalysis, 1998, 4, 776-777.	0.2	0
216	Compositional Imaging At The Sub- 2 Ã Level Using A 200 Kv Schottky Field Emission Transmission Electron Microscope. Microscopy and Microanalysis, 1998, 4, 138-139.	0.2	0

#	Article	IF	CITATIONS
217	Dispersion forces and Hamaker constants for intergranular films in silicon nitride from spatially resolved-valence electron energy loss spectrum imaging. , 1998, 46, 2271-2271.		7
218	Oxide precipitation at silicon grain boundaries. Applied Physics Letters, 1997, 70, 327-329.	1.5	14
219	The reaction between a TiNi shape memory thin film and silicon. Journal of Materials Research, 1997, 12, 1734-1740.	1.2	38
220	Improved Measurement and Analysis of Series of Valence Electron Energy Loss Spectra and The Local Electronic Structure. Microscopy and Microanalysis, 1997, 3, 943-944.	0.2	1
221	Transient Growth Bands in Silicon Nitride Cooled in Rareâ€Earthâ€Based Glass. Journal of the American Ceramic Society, 1997, 80, 1397-1404.	1.9	19
222	Amorphous SiO ₂ Precipitates at Silicon Grain Boundaries. Materials Science Forum, 1996, 207-209, 713-716.	0.3	3
223	Analyzing line scan EELS data with neural pattern recognition. Ultramicroscopy, 1995, 59, 229-239.	0.8	21
224	Interfacial Electronic Structure and Full Spectral Hamaker Constants of Si3N4 Intergranular Films from VUV and Sr-Veel Spectroscopy. Materials Research Society Symposia Proceedings, 1994, 357, 243.	0.1	5

14